JACS
JOURNAL OF THE AMERICAN CHEMICAL SOCIETY
Article
pubs.acs.org/JACS

Porous Organic Cages for Sulfur Hexafluoride Separation

Tom Hasell,[†] Marcin Miklitz,[‡] Andrew Stephenson,[†] Marc A. Little,[†] Samantha Y. Chong,[†] Rob Clowes,[†] Linjiang Chen,[†] Daniel Holden,[†] Gareth A. Tribello,[§] Kim E. Jelfs,[‡] and Andrew I. Cooper*[,†]

[†]Department of Chemistry and Centre for Materials Discovery, University of Liverpool, Crown St., Liverpool L69 7ZD, United Kingdom

[‡]Department of Chemistry, Imperial College London, South Kensington, London SW7 2AZ, United Kingdom

[§]Atomistic Simulation Centre, Department of Physics and Astronomy, Queen's University Belfast, University Road, Belfast BT7 1NN, United Kingdom

Supporting Information

ABSTRACT: A series of porous organic cages is examined for the selective adsorption of sulfur hexafluoride (SF_6) over nitrogen. Despite lacking any metal sites, a porous cage, **CC3**, shows the highest SF_6/N_2 selectivity reported for any material at ambient temperature and pressure, which translates to real separations in a gas breakthrough column. The SF_6 uptake of these materials is considerably higher than would be expected from the static pore structures. The location of SF_6 within these materials is elucidated by X-ray crystallography, and it is shown that cooperative diffusion and structural rearrangements in these molecular crystals can rationalize their superior SF_6/N_2 selectivity.

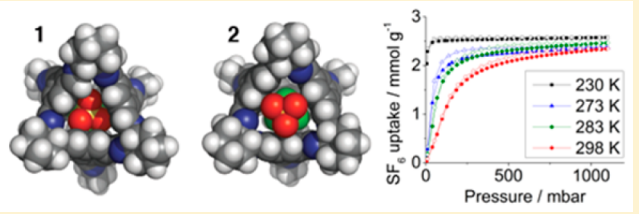

INTRODUCTION

Sulfur hexafluoride (SF_6) is a much more potent greenhouse gas than CO_2,[1,2] with an estimated atmospheric lifetime of 800−3200 years.[1] The Intergovernmental Panel on Climate Change found SF_6 to be the most potent greenhouse gas that it evaluated, with a global warming potential 23,900 times higher than CO_2.[3] Nonetheless, SF_6 has valuable and widespread industrial uses. For example, SF_6 or SF_6/N_2 mixtures are often used to insulate electrical equipment.[2,4] SF_6 is also a good thermo-acoustic insulator for windows, a contrast agent in medical applications, and a plasma etchant in the semiconductor industry.[5] There is much current interest in finding effective materials for the separation of SF_6 from gas mixtures to prevent its release into the atmosphere and to allow economically viable capture and reuse.[6] Pressure swing adsorption/desorption processes using a suitable porous material offer considerable energy savings over liquefaction, but this requires high selectivity for SF_6 adsorption over N_2 adsorption.[7] Various porous solids have been tested for SF_6 adsorption or separation[8] such as carbons,[9,10] zeolites,[11−13] metal−organic frameworks (MOFs),[5,6] and pillared clays.[14] Until now, the most selective of these materials have been zeolite 13X[12] and a series of isostructural MOFs with a high density of unsaturated metal sites.[6] The success of these materials was attributed to their pore diameters (10 and 11 Å, respectively), which were identified by Monte Carlo simulations as close to ideal.

All microporous solids tested for SF_6 separation so far have been insoluble, extended networks or macromolecules. Nitschke et al. demonstrated that a metal−organic capsule could capture and release SF_6 in solution,[27] but such molecular separation of SF_6 by a cage molecule has not yet been shown in the gas phase. However, there is also growing interest in porous molecular cages.[15−26] These cages contain an internal void that is accessible via well-defined windows, and the rigid structure of the cages prevents collapse, thus providing porosity for guest molecules. Porous organic cages have been synthesized from imines,[15−17] boronic esters,[28] and by direct carbon−carbon bond forming reactions.[29] Apparent Brunauer−Emmett−Teller (BET) surface areas for nitrogen as high as 3758 $m^2\ g^{-1}$ have been achieved.[30] Since these cages are discrete molecules, as opposed to frameworks, they are soluble in common organic solvents and can be processed into support materials and precipitated or crystallized into the solid state as required. We previously reported a class of [4 + 6] cycloimine cage compounds that show gas uptakes and physicochemical stabilities that are remarkable for molecular organic crystals.[31−33] The gas sorption properties of these cages depends both on their molecular structure, and on their crystal packing, and many of these cages can exist as multiple polymorphs.[31,34,35] These cages are excellent candidates for the molecular separation of noble gases,[36] chiral molecules,[36] and hydrocarbon isomers.[37−39] In this study, a series of these organic cages (Figure 1) was investigated for their potential in the separation of SF_6. One cage, **CC3**, shows remarkably high SF_6 selectivity, and this is related to the flexible nature of the molecular cage crystal.

Received: November 17, 2015
Published: January 13, 2016

DOI: 10.1021/jacs.5b11797
J. Am. Chem. Soc. 2016, 138, 1653−1659

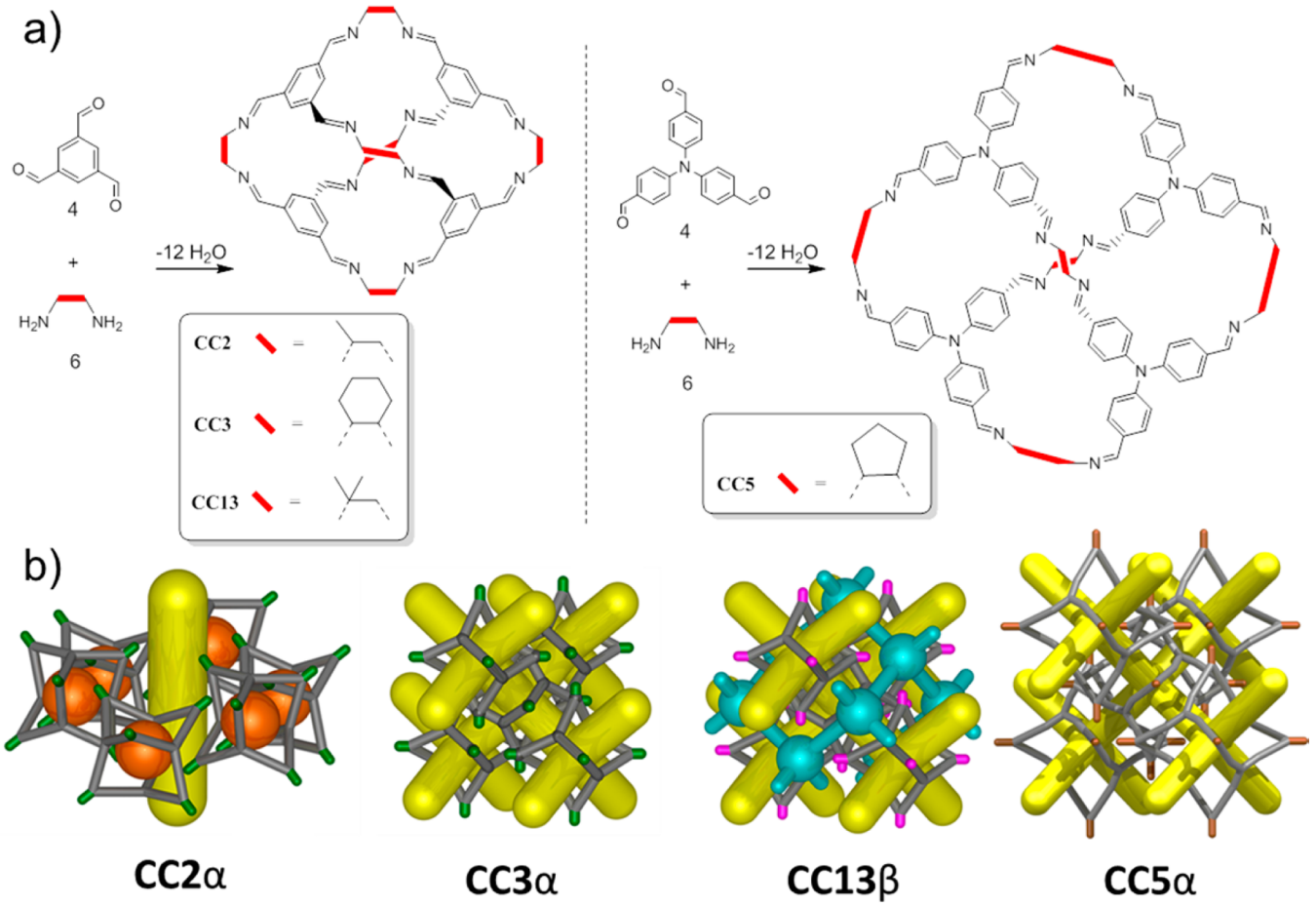

Figure 1. (a) Synthesis and structure of cages **CC1**, **CC2**, **CC5**, and **CC13**. (b) Simplified structural representations of the packing and porosity of these cages as derived from single crystal structures. **CC2***α* exhibits one-dimensional pore channels (yellow) in addition to internal cage cavities (orange), which may also be accessible depending on the size of the guest. **CC3***α* has a 3D diamondoid pore network (yellow). **CC13***β* packs with the same diamondoid pore network as **CC3***α* (running through the inside of the cages, shown in yellow), but with an additional, narrower interpenetrating diamondoid pore network between the cages (cyan). **CC5***α* packs in the same window-to-window fashion, but the cages and hence the pore channels (yellow) are larger.

METHODS

Materials and Synthesis. 1,3,5-Triformylbenzene (TFB) was purchased from Manchester Organics, UK and used as received. 2-Methyl-1,2-propanediamine was purchased from TCI Europe and used as received. All other chemicals were purchased from Sigma-Aldrich and used as received. All cages were synthesized as described previously.[31,33,40,41]

Gas Sorption Analysis. Powder samples were degassed offline at 100 °C for 15 h under dynamic vacuum (10^{-5} bar) before analysis, followed by degassing on the analysis port under vacuum, also at 100 °C. Isotherms were measured using a micromeritics 3flex surface characterization analyzer, equipped with a Cold-Edge technologies liquid helium cryostat chiller unit for temperature control.

Single Crystal Diffraction Data. Evacuated prism shaped single crystals of **CC3***α* were exposed to dry SF_6 at 1 bar pressure. The crystals of were transferred to a sample vial and after 28 h a single crystal data collection was recorded.

Single crystal X-ray data for **CC3**-*S*·$(SF_6)_{2.5}$·$(H_2O)_3$ was measured at beamline I19, Diamond Light Source, Didcot, UK using silicon double crystal monochromated synchrotron radiation (λ = 0.6889 Å, Kappa 4-circle goniometer, Rigaku Saturn724+ detector).[42] Empirical absorption corrections, using equivalent reflections, were applied by the program SADABS.[43] The structure was solved by SHELXD,[44] and refined by full-matrix least-squares on $|F|^2$ by SHELXL,[44] interfaced through the program OLEX2.[45] Absolute configuration was determined using *a priori* knowledge of the cage chirality. For full refinement details, see the Supporting Information (SI). Supplementary single crystal XRD data, including structure factors, is available free of charge from the Cambridge Crystallographic Data Centre (CCDC) via www.ccdc.cam.ac.uk/data_request/cif.

Crystal data for **CC3**-*S*·$(SF_6)_{2.5}$·$(H_2O)_3$, CCDC number CCDC 1437443: Formula $C_{144}H_{174}F_{15}N_{24}O_3S_{2.5}$; M = 2654.40 g·mol^{-1}; triclinic space group *P*1, colorless prism shaped crystal; *a* = 17.385(5), *b* = 17.425(6), *c* = 17.479(6) Å; α = 60.384(3), β = 60.308(3), γ = 60.168(3)°; *V* = 3768(2) Å^3; ρ = 1.170 g·cm^{-3}; μ = 0.108 mm^{-3}; *F* (000) = 1405; crystal size =0.13 × 0.07 × 0.07 mm^3; *T* = 100(0) K; 52 288 reflections measured (1.376 < Θ < 25.503°), 28 131 unique (R_{int} = 0.0448), 22 028 ($I > 2\sigma(I)$); R_1 = 0.0894 for observed and R_1 = 0.1091 for all reflections; wR_2 = 0.2549 for all reflections; max/min difference electron density = 0.801 and −0.923 e·Å^{-3}; data/restraints/parameters = 28 131/363/1786; GOF = 1.037. Flack parameter 0.14(4). The structure was refined with the TWINLAW [$\bar{1}$00 00$\bar{1}$ 0$\bar{1}$0] and BASF refined to 0.227(2).

Laboratory X-ray Powder Diffraction. Powder X-ray diffraction (PXRD) data were collected in transmission mode on loose powder samples held on thin Mylar film in aluminum well plates on a Panalytical X'Pert PRO MPD equipped with a high throughput screening (HTS) XYZ stage, X-ray focusing mirror, and PIXcel detector, using Cu Kα radiation. Data were measured over the range 4−50° in ∼0.013° steps over 60 min.

In Situ PXRD Gas-Loading. In situ powder diffraction data under an SF_6 atmosphere were collected at beamline I11 at Diamond Light Source using the low pressure capillary gas cell.[46] A finely ground

DOI: 10.1021/jacs.5b11797
J. Am. Chem. Soc. 2016, 138, 1653−1659

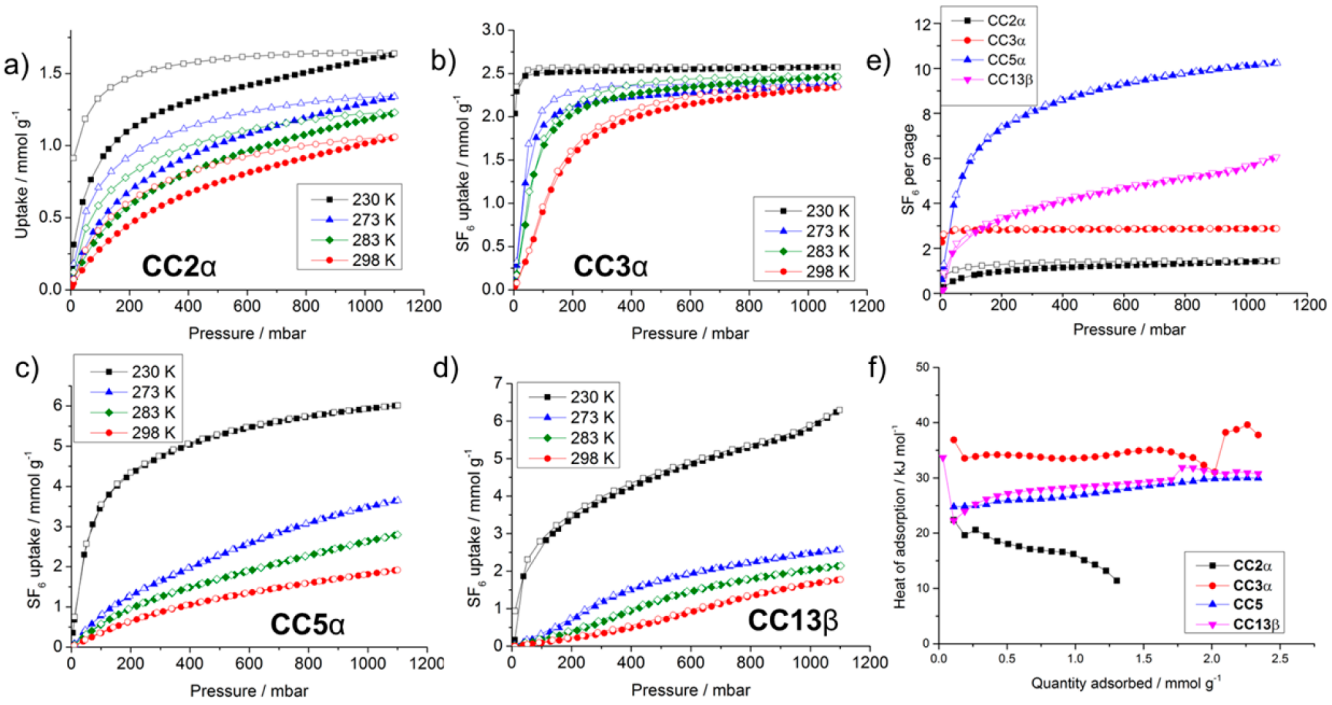

Figure 2. Gas sorption isotherms for the uptake of SF_6 in the various cages; adsorption curves shown as filled symbols, desorption curves as unfilled symbols. (a) **CC2***α*, (b) **CC3***α*, (c) **CC5***α*, and (d) **CC13***β*. (e) This plot shows the uptake expressed in terms of the number of SF_6 molecules per cage molecule at 230 K. (f) Heat of adsorption of SF_6 for the various cages.

sample of **CC13***β* was packed in a 0.7 mm diameter borosilicate capillary and mounted on the low-pressure capillary gas cell. Samples were activated by heating to 350 K using an Oxford Cryostream Plus under dynamic vacuum (approximately 10^{-5} mbar). Data were collected using the Mythen-II position sensitive detector (PSD) at 230 K. An initial powder diffraction profile of guest-free **CC13***β* was collected under dynamic vacuum. The sample was rocked through ±15° in θ to improve powder averaging. Gas was dosed into the system, initially to 2.7 bar and then 3 bar. Samples were allowed to equilibrate at both pressures for approximately of 45 min after gas was dosed into the cell. PXRD data were collected during this time to monitor equilibration. The sample was then evacuated at 373 K under dynamic vacuum and the powder profile collected to confirm removal of the guest from the pore structure.

Metadynamics Simulations. A 100 ns well-tempered metadynamics simulation was performed with DL_POLY2.20[47] and PLUMED2.[48] The OPLS-AA force field parameters,[49] and the Leapfrog Verlet algorithm[50] with a time step of 0.5 fs was used. The Nose-Hoover thermostat[51] was used to keep the temperature fixed at 300 K and no interactions were applied between periodic images in a cubic system with cell length 39 Å. A time step of 0.5 fs with sampling step of 1 ps was chosen and full molecular motion was allowed throughout the simulation. The collective variable along which the metadynamics bias was accumulated measured the distance between the center of mass of the fully flexible **CC3** and the sulfur atom of the SF_6. Gaussian hills with a width of 0.15 nm and an initial height of 1.2 kJ mol^{-1} were added every 500 MD steps and the so-called well-tempered factor was set equal to 10. The free energy surface was calculated using the "sum_hills" utility of PLUMED2 with the minimum shifted to zero. An additional well-tempered metadynamics simulation using two collective variables (the distance and a torsion angle) was performed to analyze the mechanism further; see the SI for further details.

Breakthrough Experiments. Breakthrough curves were measured for a fixed bed of **CC3***α* or zeolite 13X at 298 K using a 90:10 (v/v) N_2/SF_6 gas mixture. The breakthrough curves were measured using an automated breakthrough analyzer (manufactured by Hiden Isochema, Warrington, U.K.). **CC3***α* was made into small pellets (500−700 μm), which were packed into an adsorption bed for the breakthrough experiment. The materials were activated in situ by heating to appropriate activation temperatures and flowing helium through the column. Desorption of N_2/SF_6 was performed by flowing helium through the bed at the same flow rate as the breakthrough experiment. The effluents were measured by an in-line mass spectrometer. Further details are in the SI.

RESULTS AND DISCUSSION

Gas adsorption analyses revealed that all four cages were porous to SF_6, but with marked differences in terms of adsorption capacities that relate to their structures (Figure 2). It is interesting that SF_6 is adsorbed by the smaller cages at all: from a simple static representation of their crystal structures, SF_6 would not be expected to be able to diffuse through the pore channels of **CC2***α*, **CC3***α*, and **CC13***β*. However, these organic crystals are somewhat flexible.[52] They are composed of discrete molecules held together by weak intermolecular dispersion forces, rather than covalently bonded frameworks, and this has been shown previously to allow "porosity without pores".[53−55] Hence **CC2***α*, **CC3***α*, and **CC13***β* can adsorb SF_6, despite the fact that this gas is larger than the static window diameter in the cages. The kinetic diameter of SF_6, is 5.5 Å,[56] and thus one might not expect it to diffuse into the smaller imine cages (**CC2**, **CC3**, **CC13**) since their window diameters are ∼3.6 Å.[52] Indeed, previous unbiased MD simulations for **CC3***α* demonstrated that SF_6 did not escape the cage cavity in which it was originally positioned over a 10 ns simulation using a force field tailored to describe the flexibility in imine cages.[52] Hence, to analyze the SF_6 diffusion mechanism for these smaller cages and to calculate the energetic barrier to this event, we carried out well-tempered metadynamics simulations of SF_6 and a single **CC3** molecule (see the SI for full simulation details). To understand the diffusion mechanism, we can think of the SF_6 molecule as two connected triangular faces, rather

DOI: 10.1021/jacs.5b11797
J. Am. Chem. Soc. 2016, 138, 1653−1659

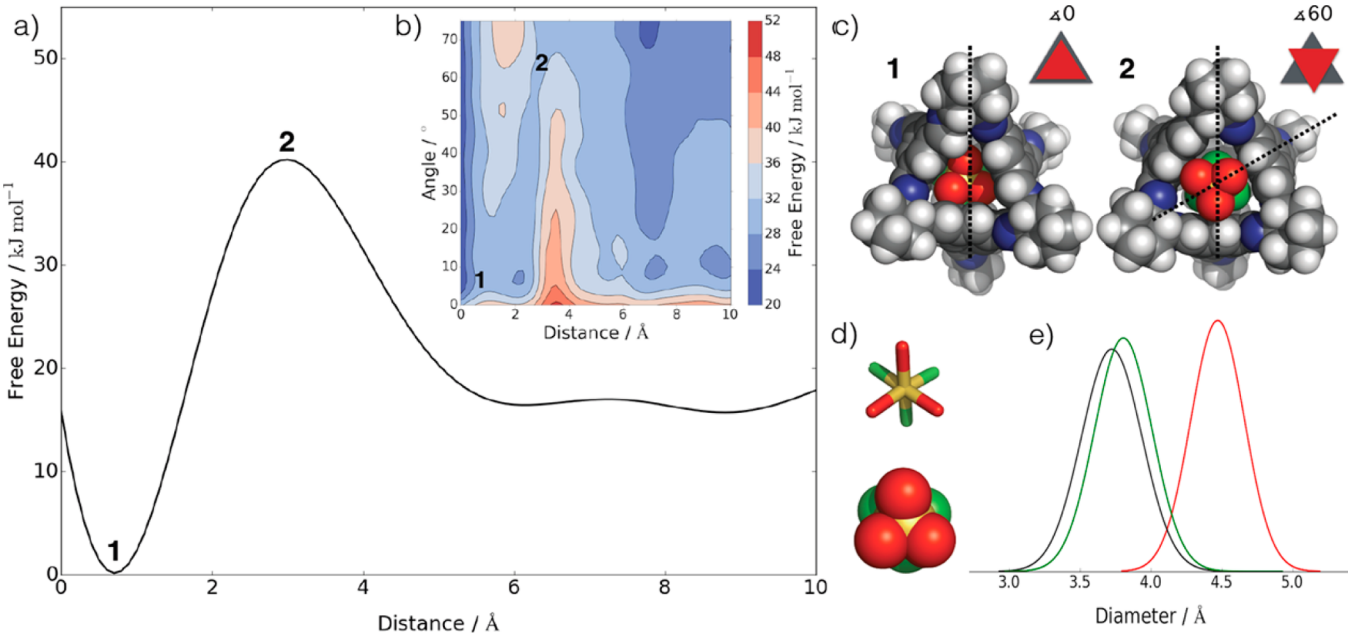

Figure 3. (a) Free energy surface for a single SF_6 molecule diffusing through the window of a single **CC3** cage as a function of the distance between the centers of mass of **CC3** and SF_6. (b) The 2D free energy as a function of the distance used for (a) and the angle of rotation as shown in part (c). (c) **CC3** and SF_6 configurations corresponding to the positions marked 1 (left) and 2 (right) on the plots. Structure 1 corresponds to the global minimum orientation with SF_6 in the **CC3** cavity, and structure 2 represents the structure at highest point of the free energy surface, when SF_6 is placed exactly in the center of the window. The angle used for the *y*-axis in panel (b) is indicated on these configurations. This angle is small when the SF_6 begins to escape from the cage and increases as the SF_6 reaches position 2. (d) Stick and spacefill representations of the SF_6 molecule. The three fluorine atoms that diffuse through the window first are colored red. (e) Comparison of the pore envelope of the **CC3** window, for an empty cage (black), for **CC3** with SF_6 occupying the cage cavity (green), and for cage where SF_6 is positioned in the window (red).

than a sphere that describes the widest possible diameter. As can be seen in Figure 3 and Movie S1, SF_6 exits the cage by first aligning its outermost triangular face with the triangular cage window. There is then a rotation of ~60° (Figure 3a–d) such that the second face can align with the cage window and thus pass through. The barrier to the SF_6 diffusion through the flexible cage window is calculated to be at most 40 kJ mol^{-1}, and the configurations near the saddle point have the center of the SF_6 traversing the window. While crystal packing effects would likely influence this barrier to a small extent, it is of similar magnitude to that previously calculated for the allowed *para*-xylene diffusion in the same host system.[37] It is therefore reasonable that the SF_6 diffuses, albeit slowly, in this system. A comparison of a single empty **CC3** window diameter distribution with the measured window diameter during the SF_6 passage (Figure 3e) reveals the cooperative character of the mechanism. Clearly, the cage window size increases when the SF_6 is inside the window.

CC3*α* shows the highest affinity for SF_6 of the four cages tested, and a steep type I isotherm that saturates at low pressures (Figure 2b). This is manifested in the highest heat of adsorption of ~35–40 kJ mol^{-1} (Figure 2f). The saturation uptake corresponds to around 2.9 SF_6 molecules per **CC3** cage (Figure 2e). This is consistent with one SF_6 molecule in the internal cage cavity, plus one SF_6 molecule shared in each of the four window–window sites surrounding every cage, equating to a maximum theoretical loading of 3 SF_6 molecules per **CC3** cage. **CC2***α* shows the lowest SF_6 uptake and the lowest heat of adsorption (Figure 2a, f). The 1D pore channels in **CC2***α*,[33] which run between the hexagonally arrayed cages, are wide enough to accommodate SF_6. The uptake of 1.4 SF_6 molecules per cage (Figure 2e) confirms that these 1D channels must be at least partially occupied. **CC5***α* displays the highest SF_6 adsorption capacity, of 10.2 SF_6 per cage, in line with its larger internal void size and its higher surface area and pore volume.[41] However, the heat of adsorption is much lower than for **CC3***α*, and hence **CC5***α* adsorbs less SF_6 at lower pressures. **CC13***β* gives a lower heat of adsorption than **CC3***α*, despite having a similar pore structure. The difference between the high temperature (298 K) and low temperature (230 K) SF_6 uptakes for **CC13***β* is significant. At 230 K, **CC13***β* adsorbs around 6 SF_6 molecules per cage—that is, twice as much gas as **CC3***α*. This can be rationalized only if the SF_6 molecules are located in the intercage sites, of which there are three per **CC13** (Figure 1b; blue nodes), as well as in the cage cavities and the window–window sites. While these intercage sites were shown previously to be accessible to nitrogen,[31] the size of the nodes relative to SF_6 suggested to us that significant rearrangement would be required to accommodate this larger gas. To explore this, the adsorption of SF_6 in **CC13***β* was monitored by PXRD (Figure 4). The PXRD pattern changes significantly as the structure is loaded with SF_6, losing intensity in the high angle range. This is consistent with the preservation of the long-range packing of the cage modules, but a more disordered local structure, which could allow the large SF_6 guest to diffuse through the crystal. This reorganization of the **CC13** structure allows the incorporation of such a large quantity of SF_6 (6 per cage), which cannot not be rationalized by the original empty structure. It is remarkable that the crystallinity is restored completely to its initial state after removal of the SF_6, even after multiple cycles (Figure S1). This behavior is allowed by the relatively weak dispersion forces between the cages, which enable reorganization in response to guests.

DOI: 10.1021/jacs.5b11797
J. Am. Chem. Soc. 2016, 138, 1653–1659

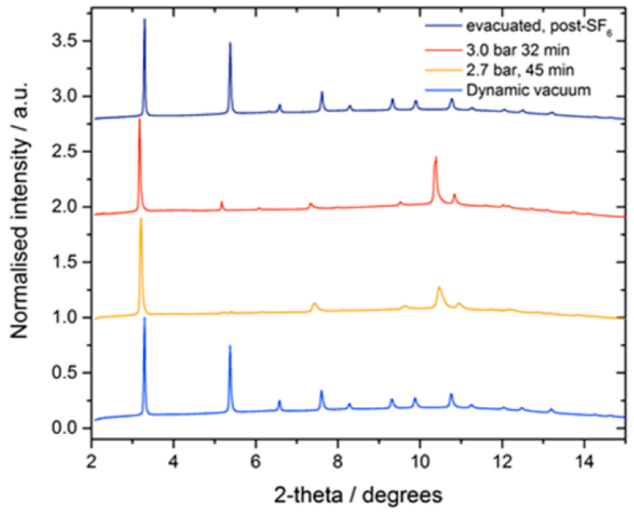

Figure 4. Powder X-ray diffraction data for in situ SF_6 loading of **CC13**β at 230 K. Under excess pressures of SF_6, the **CC13**β structure becomes more disordered at short-range, indicated by loss of high angle diffraction intensity. The original profile is totally regained after guest removal by vacuum.

The SF_6 isotherms for **CC3**α suggested excellent potential for SF_6 separation from nitrogen, and therefore the nitrogen isotherms were measured at equivalent temperatures (Figure S2) to allow the calculation of ideal adsorbed solution theory (IAST) predicted selectivity (Figures 5 and S3).[57] The

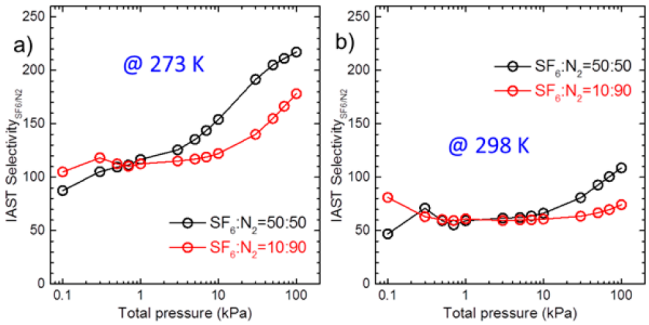

Figure 5. IAST selectivity plots for SF_6 over N_2 for **CC3**α at SF_6:N2 ratios of 50:50 and 10:90 at (a) 273 K and (b) 298 K.

industrially relevant composition for separation of an SF_6/N2 mixture is SF_6:N2 = 10%:90%.[6,12] At 1 bar pressure, **CC3**α gives a selectivity of 178 at 273 K and 74 at 298 K. This surpasses the most promising candidate material previously reported, UiO-66-Zr (selectivity = 74, at 1 bar, 293 K)[58] and other similar framework materials such as Zn-MOF-74 (selectivity = 46, at 1 bar, 298 K),[6] Ca-A zeolite (28 at 1 bar, 298 K),[13] and zeolite-13X (44 at 1 bar, 298 K).[12] The total capacity of **CC3**α for SF_6 is higher than that of many of the frameworks reported (e.g., UiO-66-Zr is ~1.5 mmol, at 293 K and 1 bar), but lower than that of the highest (Mg-MOF-74 = 6.42 mmol g^{-1} at 1 bar, 298 K).

A crystallographic study allowed for the location of SF_6 in **CC3**α to be accurately determined (Figures 6 and S4). Well-ordered SF_6 molecules were located, with full site occupancies, in the intrinsic **CC3** cavities (Figure S4). **CC3** provides an ideal fit for SF_6 in terms of both size and geometry of the cage cavity (Figure 6), which explains the high heat of adsorption that we observe. The ordering of SF_6 molecules in the **CC3** cavities

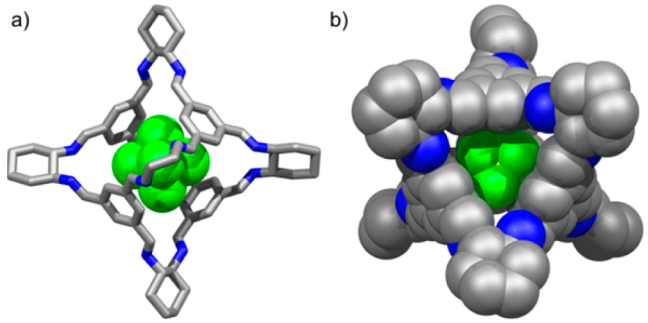

Figure 6. (a) Resolved position of SF_6 in the **CC3** cavity determined from the single crystal structure; (b) space filling representation as viewed through a cage window.

transforms the crystallographic symmetry from $F4_132$, as determined for the empty **CC3**α host, to $P1$, but this does not alter the crystal packing of the **CC3** molecules.

IAST calculations are useful to suggest selectivity in a separation of two or more gases for an adsorptive separation process, but IAST does not accurately represent a gas mixture flowing through a packed bed of material.[58] In particular, IAST calculations say little about separation kinetics since the calculations are derived from single-component gas sorption isotherms that are collected at thermodynamic equilibrium. Therefore, breakthrough experiments were carried out to establish the practical potential of **CC3**α for N_2/SF_6 separations, and in particular to demonstrate that the SF_6 diffusion kinetics are sufficiently fast for real separations. All breakthrough experiments were performed at 298 K with a 90:10 (v/v) N_2/SF_6 mixture. The breakthrough curves and desorption curves for N_2 and SF_6 flowing through a bed of **CC3**α are shown in Figure 7. The selectivity determined from

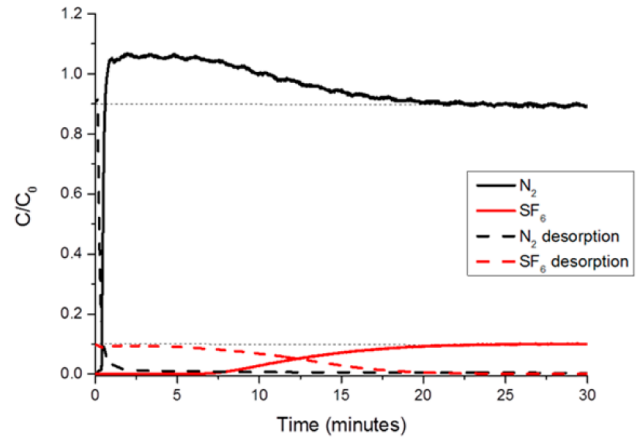

Figure 7. N_2/SF_6 (90:10) breakthrough curve for **CC3**α at 298 K. Total flow rate was 25 mL min^{-1}, and pressure was 1 bar. Desorption was performed by flowing helium through the bed at the same flow rate and pressure.

the relative uptake capacities is 76.5, in good agreement with the IAST calculations. Nitrogen breaks through the column within 1 min, whereas SF_6 does not start to break through until after 6.5 min and does not completely break through until approximately 20 min. The large difference in breakthrough time between N_2 and SF_6 reflects the much higher affinity of **CC3**α toward SF_6. The breakthrough curve for N_2 shows the characteristic "roll-up" as the concentration at the outlet is

DOI: 10.1021/jacs.5b11797
J. Am. Chem. Soc. 2016, 138, 1653−1659

temporarily higher than at the inlet as the SF_6 is preferentially adsorbed and displaces the N_2. The desorption was performed by flowing helium through the column under the same conditions as for breakthrough. N_2 is desorbed quickly from the column, with 97% of the gas being desorbed within the first minute. As expected, SF_6 is desorbed more slowly, with full desorption taking about 20 min, approximately the same time as for full breakthrough.

Breakthrough and desorption curves for **CC3**α and zeolite 13X at three different gas flow rates are compared in Figures S5 and S6. In each case, the desorption of SF_6 from **CC3** takes approximately the same time as the full breakthrough. However, for zeolite 13X with a 25 mL min^{-1} flow rate, SF_6 desorption takes twice as long as it does to breakthrough (Figure S6). The more rapid desorption efficiency of **CC3**α therefore gives it a potential advantage over zeolite 13X as a material for N_2/SF_6 separation.[59]

SUMMARY

Intrinsically porous molecules, as opposed to framework or network materials, have been investigated for SF_6 uptake separation. Despite the pore limiting diameters in **CC3**α being considerably narrower[36,52] than the 11 Å recommended as the optimum pore size by simulation,[60] this cage shows unprecedented selectivity for SF_6 over N_2. Our simulations suggest this may be a result of the flexibility of the **CC3**α molecular crystal, which allows SF_6 to diffuse by cooperative effects, before the structure relaxes back to produce a closer, near-ideal interaction with the SF_6 guest. This hypothesis is further supported by research reported by Camp and Sholl while this Article was being written.[61] In that study, transition state theory methods were used to simulate the diffusion of various gases in **CC3**α, and it was found for SF_6 that no diffusion would be expected in a static system, while diffusion should be possible if the flexibility of the host is taken into account. The IAST selectivity of **CC3**α for an industrially relevant mixture of 10:90 SF_6:N_2 at 298 K and 1 bar is higher than that of other reported materials. Breakthrough experiments confirmed that **CC3**α is effective for separation of N_2 and SF_6. Also, desorption curves show that SF_6 is more efficiently desorbed from **CC3**α than from zeolite 13X. Flexibility in MOFs has been found to provide higher gas capacities.[62] Similarly, the flexibility of molecular crystals, such as **CC3**α, allows for a stronger gas binding with SF_6, which gives these materials potential for practical gas separations under flow.

ASSOCIATED CONTENT

Supporting Information

The Supporting Information is available free of charge on the ACS Publications website at DOI: 10.1021/jacs.5b11797.

Crystallographic details, analysis equipment and conditions, and further characterization details (PDF)

CC3 SF_6 crystallographic data (CIF)

Example of the mechanism via which the SF_6 molecule diffuses through one of the four **CC3** windows from the internal cavity of **CC3** to the exterior (MPG)

AUTHOR INFORMATION

Corresponding Author

*aicooper@liv.ac.uk

Notes

The authors declare no competing financial interest.

ACKNOWLEDGMENTS

We thank the Engineering and Physical Sciences Research Council (EP/H000925/1 and EP/K018396/1) and the European Research Council under FP7 (RobOT, ERC Grant Agreement No. 321156). T.H. and K.E.J. are Royal Society University Research Fellows. We thank the STFC for access to Diamond Light Source and the staff at beamlines I19 (MT8728) and I11 (EE9282), and Drs. C. Murray and A. Baker for help with gas cell experiments.

REFERENCES

(1) Ravishankara, A. R.; Solomon, S.; Turnipseed, A. A.; Warren, R. F. *Science* **1993**, *259*, 194.
(2) Fang, X.; Hu, X.; Janssens-Maenhout, G.; Wu, J.; Han, J.; Su, S.; Zhang, J.; Hu, J. *Environ. Sci. Technol.* **2013**, *47*, 3848.
(3) Solomon, S.; Qin, D.; Manning, M. *Technical Summary*; Cambridge University Press: New York, 2007.
(4) Christophorou, L. G.; Vanbrunt, R. J. *IEEE Trans. Dielectr. Electr. Insul.* **1995**, *2*, 952.
(5) Senkovska, I.; Barea, E.; Rodriguez Navarro, J. A.; Kaskel, S. *Microporous Mesoporous Mater.* **2012**, *156*, 115.
(6) Kim, M.-B.; Lee, S.-J.; Lee, C. Y.; Bae, Y.-S. *Microporous Mesoporous Mater.* **2014**, *190*, 356.
(7) Yang, R. T. In *Adsorbents: Fundamentals and Applications*; John Wiley & Sons, Inc: Hoboken, NJ, 2003; p 17.
(8) Cao, D. V.; Sircar, S. *Adsorption* **2001**, *7*, 73.
(9) Cho, W.-S.; Lee, K.-H.; Chang, H.-J.; Huh, W.; Kwon, H.-H. *Korean J. Chem. Eng.* **2011**, *28*, 2196.
(10) Chiang, Y.-C.; Wu, P.-Y. *J. Hazard. Mater.* **2010**, *178*, 729.
(11) Cao, D. V.; Sircar, S. *Ind. Eng. Chem. Res.* **2001**, *40*, 156.
(12) Murase, H.; Imai, T.; Inohara, T.; Toyoda, M. *IEEE Trans. Dielectr. Electr. Insul.* **2004**, *11*, 166.
(13) Toyoda, M.; Murase, H.; Imai, T.; Naotsuka, H.; Kobayashi, A.; Takano, K.; Ohkuma, K. *IEEE Trans. Power Delivery* **2003**, *18*, 442.
(14) Bandosz, T. J.; Jagiello, J.; Schwarz, J. A. *J. Chem. Eng. Data* **1996**, *41*, 880.
(15) Holst, J. R.; Trewin, A.; Cooper, A. I. *Nat. Chem.* **2010**, *2*, 915.
(16) Tian, J.; Thallapally, P. K.; McGrail, B. P. *CrystEngComm* **2012**, *14*, 1909.
(17) Zhang, G.; Mastalerz, M. *Chem. Soc. Rev.* **2014**, *43*, 1934.
(18) Slater, A. G.; Cooper, A. I. *Science* **2015**, *348*, aaa8075.
(19) Jin, Y. H.; Wang, Q.; Taynton, P.; Zhang, W. *Acc. Chem. Res.* **2014**, *47*, 1575.
(20) Ding, H.; Yang, Y.; Li, B.; Pan, F.; Zhu, G.; Zeller, M.; Yuan, D.; Wang, C. *Chem. Commun.* **2015**, *51*, 1976.
(21) Wang, Q.; Zhang, C. X.; Noll, B. C.; Long, H.; Jin, Y. H.; Zhang, W. *Angew. Chem., Int. Ed.* **2014**, *53*, 10663.
(22) Zhang, C.; Chen, C. F. *J. Org. Chem.* **2007**, *72*, 9339.
(23) Zhang, C.; Wang, Z.; Tan, L.; Zhai, T.-L.; Wang, S.; Tan, B.; Zheng, Y.-S.; Yang, X.-L.; Xu, H.-B. *Angew. Chem., Int. Ed.* **2015**, *54*, 9244.
(24) Evans, J. D.; Sumby, C. J.; Doonan, C. J. *Chem. Lett.* **2015**, *44*, 582.
(25) Mastalerz, M.; Oppel, I. M. *Angew. Chem., Int. Ed.* **2012**, *51*, 5252.
(26) Schneider, M. W.; Hauswald, H. J. S.; Stoll, R.; Mastalerz, M. *Chem. Commun.* **2012**, *48*, 9861.
(27) Riddell, I. A.; Smulders, M. M. J.; Clegg, J. K.; Nitschke, J. R. *Chem. Commun.* **2011**, *47*, 457.
(28) Mastalerz, M. *Angew. Chem., Int. Ed.* **2010**, *49*, 5042.
(29) Avellaneda, A.; Valente, P.; Burgun, A.; Evans, J. D.; Markwell-Heys, A. W.; Rankine, D.; Nielsen, D. J.; Hill, M. R.; Sumby, C. J.; Doonan, C. J. *Angew. Chem., Int. Ed.* **2013**, *52*, 3746.

DOI: 10.1021/jacs.5b11797
J. Am. Chem. Soc. 2016, 138, 1653−1659

(30) Zhang, G.; Presly, O.; White, F.; Oppel, I. M.; Mastalerz, M. *Angew. Chem., Int. Ed.* **2014**, *53*, 1516.
(31) Hasell, T.; Culshaw, J. L.; Chong, S. Y.; Schmidtmann, M.; Little, M. A.; Jelfs, K. E.; Pyzer-Knapp, E. O.; Shepherd, H.; Adams, D. J.; Day, G. M.; Cooper, A. I. *J. Am. Chem. Soc.* **2014**, *136*, 1438.
(32) Mitra, T.; Wu, X.; Clowes, R.; Jones, J. T. A.; Jelfs, K. E.; Adams, D. J.; Trewin, A.; Bacsa, J.; Steiner, A.; Cooper, A. I. *Chem. - Eur. J.* **2011**, *17*, 10235.
(33) Tozawa, T.; Jones, J. T. A.; Swamy, S. I.; Jiang, S.; Adams, D. J.; Shakespeare, S.; Clowes, R.; Bradshaw, D.; Hasell, T.; Chong, S. Y.; Tang, C.; Thompson, S.; Parker, J.; Trewin, A.; Bacsa, J.; Slawin, A. M. Z.; Steiner, A.; Cooper, A. I. *Nat. Mater.* **2009**, *8*, 973.
(34) Jones, J. T. A.; Holden, D.; Mitra, T.; Hasell, T.; Adams, D. J.; Jelfs, K. E.; Trewin, A.; Willock, D. J.; Day, G. M.; Bacsa, J.; Steiner, A.; Cooper, A. I. *Angew. Chem., Int. Ed.* **2011**, *50*, 749.
(35) Little, M. A.; Chong, S. Y.; Schmidtmann, M.; Hasell, T.; Cooper, A. I. *Chem. Commun.* **2014**, *50*, 9465.
(36) Chen, L.; Reiss, P. S.; Chong, S. Y.; Holden, D.; Jelfs, K. E.; Hasell, T.; Little, M. A.; Kewley, A.; Briggs, M. E.; Stephenson, A.; Thomas, K. M.; Armstrong, J. A.; Bell, J.; Busto, J.; Noel, R.; Liu, J.; Strachan, D. M.; Thallapally, P. K.; Cooper, A. I. *Nat. Mater.* **2014**, *13*, 954.
(37) Mitra, T.; Jelfs, K. E.; Schmidtmann, M.; Ahmed, A.; Chong, S. Y.; Adams, D. J.; Cooper, A. I. *Nat. Chem.* **2013**, *5*, 276.
(38) Kewley, A.; Stephenson, A.; Chen, L. J.; Briggs, M. E.; Hasell, T.; Cooper, A. I. *Chem. Mater.* **2015**, *27*, 3207.
(39) Zhang, J.-H.; Xie, S.-M.; Chen, L.; Wang, B.-J.; He, P.-G.; Yuan, L.-M. *Anal. Chem.* **2015**, *87*, 7817.
(40) Hasell, T.; Chong, S. Y.; Jelfs, K. E.; Adams, D. J.; Cooper, A. I. *J. Am. Chem. Soc.* **2012**, *134*, 588.
(41) Jones, J. T. A.; Hasell, T.; Wu, X.; Bacsa, J.; Jelfs, K. E.; Schmidtmann, M.; Chong, S. Y.; Adams, D. J.; Trewin, A.; Schiffman, F.; Cora, F.; Slater, B.; Steiner, A.; Day, G. M.; Cooper, A. I. *Nature* **2011**, *474*, 367.
(42) Nowell, H.; Barnett, S. A.; Christensen, K. E.; Teat, S. J.; Allan, D. R. *J. Synchrotron Radiat.* **2012**, *19*, 435.
(43) Sheldrick, G. M. *SADABS*; University of Göttingen, Göttingen, Germany, 2008.
(44) Sheldrick, G. M. *Acta Crystallogr., Sect. A: Found. Crystallogr.* **2008**, *64*, 112.
(45) Dolomanov, O. V.; Bourhis, L. J.; Gildea, R. J.; Howard, J. A. K.; Puschmann, H. *J. Appl. Crystallogr.* **2009**, *42*, 339.
(46) Parker, J. E.; Potter, J.; Thompson, S. P.; Lennie, A. R.; Tang, C. C. *Mater. Sci. Forum* **2012**, *706–709*, 1707–1712.
(47) Smith, W.; Yong, C. W.; Rodger, P. M. *Mol. Simul.* **2002**, *28*, 385–471.
(48) Tribello, G.; Bonomi, M.; Branduardi, D.; Camilloni, C.; Bussi, G. *Comput. Phys. Commun.* **2014**, *185*, 604.
(49) Jorgensen, W. L.; Maxwell, D. S.; Tirado-Rives, J. *J. Am. Chem. Soc.* **1996**, *118*, 11225–11236.
(50) Hockney, R. W. *Methods Comput. Phys.* **1970**, *9*, 135.
(51) Hoover, W. G. *Phys. Rev. A: At., Mol., Opt. Phys.* **1985**, *31*, 1695.
(52) Holden, D.; Jelfs, K. E.; Trewin, A.; Willock, D. J.; Haranczyk, M.; Cooper, A. I. *J. Phys. Chem. C* **2014**, *118*, 12734.
(53) Barbour, L. J. *Chem. Commun.* **2006**, 1163.
(54) Dobrzanska, L.; Lloyd, G. O.; Raubenheimer, H. G.; Barbour, L. J. *J. Am. Chem. Soc.* **2006**, *128*, 698.
(55) Herbert, S. A.; Janiak, A.; Thallapally, P. K.; Atwood, J. L.; Barbour, L. J. *Chem. Commun.* **2014**, *50*, 15509.
(56) Breck, D. In *Molecular Sieve Zeolites-I*; Flanigen, E. M., Sand, L. B., Eds.; American Chemical Society: Washington, DC, 1974; Vol. *101*, p 1, DOI: 10.1021/ba-1971-0101.ch001.
(57) Myers, A. L.; Prausnitz, J. M. *AIChE J.* **1965**, *11*, 121.
(58) Kim, M.-B.; Yoon, T.-U.; Hong, D.-Y.; Kim, S.-Y.; Lee, S.-J.; Kim, S.-I.; Lee, S.-K.; Chang, J.-S.; Bae, Y.-S. *Chem. Eng. J.* **2015**, *276*, 315.
(59) Kim, P.-J.; You, Y.-W.; Park, H.; Chang, J.-S.; Bae, Y.-S.; Lee, C.-H.; Suh, J.-K. *Chem. Eng. J.* **2015**, *262*, 683.
(60) Builes, S.; Roussel, T.; Vega, L. F. *AIChE J.* **2011**, *57*, 962.
(61) Camp, J. S.; Sholl, D. S. *J. Phys. Chem. C* **2015**, DOI: 10.1021/acs.jpcc.5b11111.
(62) Mason, J. A.; Oktawiec, J.; Taylor, M. K.; Hudson, M. R.; Rodriguez, J.; Bachman, J. E.; Gonzalez, M. I.; Cervellino, A.; Guagliardi, A.; Brown, C. M.; Llewellyn, P. L.; Masciocchi, N.; Long, J. R. *Nature* **2015**, *527*, 357–361.

DOI: 10.1021/jacs.5b11797
J. Am. Chem. Soc. 2016, 138, 1653–1659